Prediction of two-dimensional topological insulator by forming a surface alloy on Au/Si(111) substrate

Feng-Chuan Chuang, Chia-Hsiu Hsu, Hsin-Lei Chou, Christian P. Crisostomo, Zhi-Quan Huang, Shih-Yu Wu, and Chien-Cheng Kuo*
Department of Physics, National Sun Yat-Sen University, Kaohsiung 804, Taiwan

Wang-Chi V. Yeh
Department of Physics, National Dong Hwa University, Hualien 97401, Taiwan

Hsin Lin†
Centre for Advanced 2D Materials and Graphene Research Centre, National University of Singapore, Singapore 117546, Singapore and Department of Physics, National University of Singapore, Singapore 117542, Singapore

Arun Bansil
Department of Physics, Northeastern University, Boston, Massachusetts 02115, USA
(Received 11 September 2015; revised manuscript received 22 December 2015; published 19 January 2016)

Two-dimensional (2D) topological insulators (TIs), which can be integrated into the modern silicon industry, are highly desirable for spintronics applications. Here, using first-principles electronic structure calculations, we show that the Au/Si(111)-$\sqrt{3}$ substrate can provide a platform for hosting 2D TIs obtained through the formation of surface alloys with a honeycomb pattern of adsorbed atoms. We systematically examined elements from groups III to VI of the periodic table at 2/3 monolayer coverage on Au/Si(111)-$\sqrt{3}$, and found that In, Tl, Ge, and Sn adsorbates result in topologically nontrivial phases with band gaps varying from 0 to 50 meV. Our scanning tunneling microscopy and low-energy electron diffraction experiments confirm the presence of the honeycomb pattern when Bi atoms are deposited on Au/Si(111)-$\sqrt{3}$, in accord with our theoretical predictions. Our findings pave the way for using surface alloys as a potential route for obtaining viable 2D TI platforms.

DOI: 10.1103/PhysRevB.93.035429

I. INTRODUCTION

Two-dimensional (2D) topological insulators (TIs), also known as quantum spin Hall (QSH) insulators, are recently discovered novel materials in which, even though the bulk material is insulating, the system still supports spin-polarized, gapless edge states with Dirac-cone-like linear energy dispersion [1]. The robustness of these edge states against nonmagnetic impurities makes them especially well suited for spintronics applications. The experimental demonstration of the existence of topological spin transport channels, however, is currently limited to quantum wells [2–6] with band gaps too small for room-temperature applications. The search for new classes of 2D TI materials with large band gaps has thus become a challenge of urgent importance.

Recent theoretical studies predict that thin films of elements of groups IV, V, and III-V alloys, including carbon [7], silicon [8], germanium [9], tin [10], bismuth [11], InBi, GaBi, and TlBi [12], can harbor 2D TI phases in their equilibrium honeycomb structures. This is also the case for strained arsenic [13], antimony [14], BBi, and AlBi [12] honeycombs. Following the successful prediction [15] and synthesis [16] of hydrogenated graphene (or graphane), chemical adsorption on honeycombs has been considered for growing suitable nanoscale materials. Accordingly, the effects of hydrogen and halogen adsorption on the electronic and topological properties of a variety of films have been explored [17–26].

Many newly identified 2D TIs [10–12,14,21–28] have band gaps that exceed thermal energy at room temperature. However, for practical applications, a freestanding 2D TI must be placed or grown on a substrate which, in general, would result in charge transfer between the film and the substrate and modify the atomic structure and alter band topologies [22,28,29]. Substantial substrate-induced effects in experimental attempts to grow bismuth films [11,30–37] have, for example, been encountered. Another theoretical approach that has been taken is to consider placing heavy metal elements such as Bi with large spin-orbit coupling (SOC) on Si(111)-$\sqrt{3} \times \sqrt{3}$-X (X = H, Cl, Br, I) [38,39] and SiC(0001) [22], where nontrivial substrate-induced TI phases are predicted as the p_z bands are removed from the Fermi level. However, the well-known Bi trimer will likely form on Si(111) due to a strong Bi-Bi interaction [29,40–42]. On the other hand, Au on Si(111) is an existing metallic system with large spin splitting due to Au. But the possibility of tailoring nontrivial topological phases on this substrate, to our knowledge, has yet to be explored in the literature, although the formation of a well-ordered surface alloy when In atoms are deposited on Au/Si(111)-$\sqrt{3}$ [43–47] has been reported.

In this paper, using first-principles electronic structure calculations, we systematically examine the effects of 2/3 monolayer (ML) coverage on an Au/Si(111)-$\sqrt{3}$ substrate using groups III to VI elements. In, Tl, Ge, and Sn adsorbates are found to yield 2D TI phases with band gaps varying from

*cckuo@mail.nsysu.edu.tw
†nilnish@gmail.com

0 to 50 meV. For Bi adsorption, two different structural models are investigated in detail: a planar and a buckled Bi honeycomb layer. A large-gap TI phase is predicted for the planar structure, but in the buckled structure, the Z_2 trivial phase is found to have a slightly lower total energy. We have also carried out scanning tunneling microscopy and low-energy electron diffraction experiments in films obtained by 2/3 ML deposition of Bi on Au/Si(111)-$\sqrt{3}$. These measurements reveal the formation of a buckled honeycomb pattern, which is consistent with our structural predictions.

II. METHODS

The first-principles calculations were carried out within the generalized gradient approximation (GGA) [48] to the density functional theory [49] using projector-augmented-wave potentials [50], as implemented in the Vienna *ab initio* simulation package (VASP) [51]. The kinetic energy cutoff was set at 500 eV. We employed a periodically repeating slab consisting of four Si bilayers, a reconstructed layer, and a vacuum space of ∼20 Å. Hydrogen atoms were used to passivate the Si dangling bonds at the bottom of the slab. Silicon atoms of the bottom bilayer were kept fixed at the bulk crystalline positions corresponding to the theoretical Si lattice constant of 5.468 Å. The remaining Si, Au, and adsorbed atoms were relaxed until the residual force on each atom was smaller than 0.01 eV/Å. The Γ-centered $10 \times 10 \times 1$ Monkhorst-Pack [52] grid was used to sample the surface Brillouin zones (SBZs) for the $\sqrt{3}$ phases. Spin-orbit coupling was included in band structure calculations. In order to identify the topology of the band structures, we followed the method of Ref. [53] for calculating the Z_2 invariant in terms of the so-called n-field configuration of the system.

Concerning experimental details, the Bi structure on Au/Si(111)-$\sqrt{3}$ [Si(111)-α-$\sqrt{3} \times \sqrt{3}$-Au] was grown in an ultrahigh vacuum system (1×10^{-10} Torr base pressure) equipped for low-energy electron diffraction (LEED) and scanning tunneling microscopy/spectroscopy (STM/STS) measurements. A clean Si(111) substrate was obtained by flashing the sample at ∼1200 °C. The Au/Si(111)-$\sqrt{3}$ surface was prepared by depositing Au on clean Si(111) with temperature held at ∼500 °C, which was then slowly cooled back to room temperature after Au deposition. The amount of Au was determined by continuously depositing Au until a clear LEED and STM pattern for Au/Si(111)-$\sqrt{3}$ was observed. A 0.66 ML Bi was then deposited on the surface at room temperature, followed by annealing to ∼280 °C. The deposition rate of Bi (0.26 ML/min) was calibrated earlier by observing the 1×8 and 1×4 Bi/Au(110) surface [54]. LEED and STM measurements were performed *in situ* to characterize the surface structure. The operation of STM was at 78 K with a tungsten tip.

III. RESULTS AND DISCUSSION

We start by noting that we have previously examined numerous possible configurations [46] for metals adsorbed on Au/Si(111) and identified two low-energy models, which are shown in Fig. 1. (Other combinations of adsorbed sites yield structures with higher energies.) Figure 1 shows the

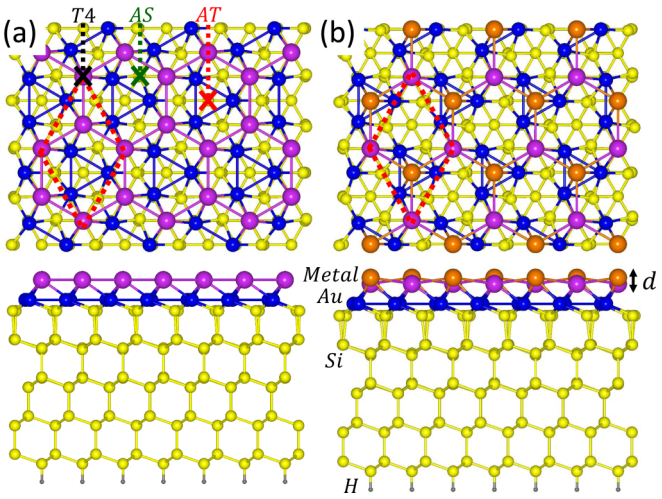

FIG. 1. Side and top views of two structural models used for metal adsorbates on an Au/Si(111)-$\sqrt{3}$ substrate: (a) planar and (b) buckled honeycomb. The orange colored atoms are placed slightly higher than the purple colored atoms. The red dashed line marks the unit cell of the $\sqrt{3}$ structure.

top and side views of the crystal structure of group III to VI nonmagnetic (metallic) elements in planar and buckled honeycombs on an Au/Si(111)-$\sqrt{3}$ substrate. In Fig. 1(a), the two adsorbed atoms in the unit cell reside at positions higher than the Au atoms and lie right on top of the T4 site with respect to the underlying Si(111) substrate, and for this reason we refer to this structure as the T4-T4 (or 2T4) model. The surface alloy shows a planar honeycomb pattern with a lattice constant of 6.70 Å on Au/Si(111)-$\sqrt{3}$, and remains planar when the two adsorbed atoms are at T4 sites. This model is the lowest-energy model for group III, IV, and VI adsorbates. However, we find that a buckled honeycomb with a vertical distance $d = 0.5$ Å has a slightly lower energy compared to the planar honeycomb for adsorbates of group V [see Fig. 1(b)]. Here, also the two adsorbates occupy T4 sites as in Fig. 1(a), but the trimer distances are altered.

The key features of the band structures and band topologies resulting from the adsorption of various atoms are summarized in Table I. The system band gap here is defined as the energy difference between the bottom of the conduction band and the top of the valence band, $\Delta E_{\text{gap}} = E_{\text{conduction}} - E_{\text{valence}}$. (Note that in general this gap is not a direct gap.) A positive value of ΔE_{gap} implies that the system is an insulator or a semiconductor, while a negative value indicates a semimetal or metallic state. A few representative band structures (including SOC) for adsorbates from groups III-VI elements are shown in Fig. 2; the blue and red circles denote bands for spin orientation projected along $-k_y$ and $+k_y$ axis, respectively. Under group III, four elements (Al, Ga, In, and Tl) yield the lowest-energy crystal structure shown in Fig. 1(a), with Al and Ga leading to semimetals, while In and Tl result in insulators with nontrivial band topologies. The band structure of Tl adsorbed on Au/Si(111)-$\sqrt{3}$ exhibits a band gap of 50 meV [see Fig. 2(a)]. The band structure for In adsorbates is similar, although with a smaller band gap of 41 meV. Group IV elements also adopt the planar honeycomb structure of

TABLE I. The band gap and Z_2 invariant for different adsorbed atoms for the chained honeycomb trimer (CHCT) model. The adsorbed atoms in the structural model of Fig. 1(a) are in planar (PL) locations, while in the model of Fig. 1(b) they are in buckled (BK) positions. d denotes the vertical distance of the buckled metal layer in Å. ΔE_{gap} is the system wide gap defined as the difference between the bottom of the conduction band and the top of the valence band. Positive values of ΔE_{gap} imply a semiconducting/insulating state, while a negative value leads to a semimetal/metal state.

Group	Element	Model	State	ΔE_{gap} (eV)	Z_2	d
III	Al	PL [Fig. 1(a)]	Semimetal	−0.139	0	
III	Ga	PL [Fig. 1(a)]	Semimetal	−0.092	0	
III	In	PL [Fig. 1(a)]	Insulator	0.041	1	
III	Tl	PL [Fig. 1(a)]	Insulator	0.050	1	
IV	Ge	PL [Fig. 1(a)]	Semimetal	−0.051	1	
IV	Sn	PL [Fig. 1(a)]	Semimetal	−0.046	1	
IV	Pb	PL [Fig. 1(a)]	Metal	Metal	Metal	
V	As	PL [Fig. 1(a)]	Semimetal	−0.106	0	
V	As	BK [Fig. 1(b)]	Insulator	0.047	0	0.343
V	Sb	PL [Fig. 1(a)]	Semimetal	−0.024	1	
V	Sb	BK [Fig. 1(b)]	Insulator	0.321	0	0.474
V	Bi	PL [Fig. 1(a)]	Insulator	0.194	1	
V	Bi	BK [Fig. 1(b)]	Semimetal	−0.072	0	0.507
VI	Se	PL [Fig. 1(a)]	Insulator	0.933	0	
VI	Te	PL [Fig. 1(a)]	Insulator	0.596	0	

Fig. 1(a), with Pb yielding a metallic state and Ge and Sn giving a nontrivial semimetal phase. The band structure for the case of Sn is shown in Fig. 2(b). Turning to group V elements, two low-energy models (planar and buckled) were examined. For the planar case [Fig. 1(a)], we obtain a trivial semimetal for As and a nontrivial semimetal for Sb. Bi with a stronger SOC strength, however, yields a nontrivial insulator with a band gap of 194 meV [see Fig. 2(c)]. Notably, for all three elements (As, Sb, and Bi) the model with a buckled pattern has a slightly lower energy (e.g., 60 meV per $\sqrt{3}$ supercell for Bi) with a trivial band topology. Finally, among the group VI elements, Se and Te both result in trivial insulators; the band structure for the Te case is shown in Fig. 2(d).

We have assessed the robustness of our results by carrying out test computations based on the Heyd-Scuseria-Ernzerhof hybrid functional HSE06 [55]. For this purpose, we considered two models for Bi on Au/Si(111) [Figs. 1(a) and 1(b)], and found the resulting HSE06 based Z_2 values to be consistent with the corresponding GGA based results given in Table I.

In order to gain further insight into the nontrivial band topologies resulting from adsorbed atoms on Au/Si(111)-$\sqrt{3}$, we have carried out edge state calculations. Here, we took Bi adsorbates as the exemplar system since Bi yields the largest band gap for the planar model of Fig. 1(a) among all the systems we considered. For this purpose, we constructed a 36.87 Å ($4\sqrt{3} \times a$) Bi-adsorbed ribbon with zigzag edges [see Fig. 3(a)]. In the region without Bi, the top surface is

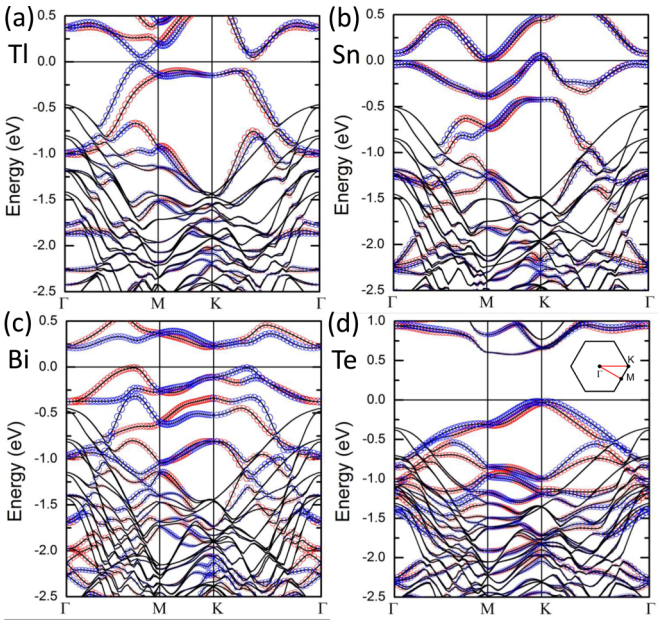

FIG. 2. Representative band structures for adsorbates from groups III-VI on an Au/Si(111)-$\sqrt{3}$ substrate, assuming the planar honeycomb structure of Fig. 1(a): (a) Tl (group III), (b) Sn (group IV), (c) Bi (group V), and (d) Te (group VI). Red and blue circles identify metal-derived states with opposite spins. A 2D Brillouin zone of Au/Si(111)-$\sqrt{3}$ with specific symmetry points labeled is shown in (d).

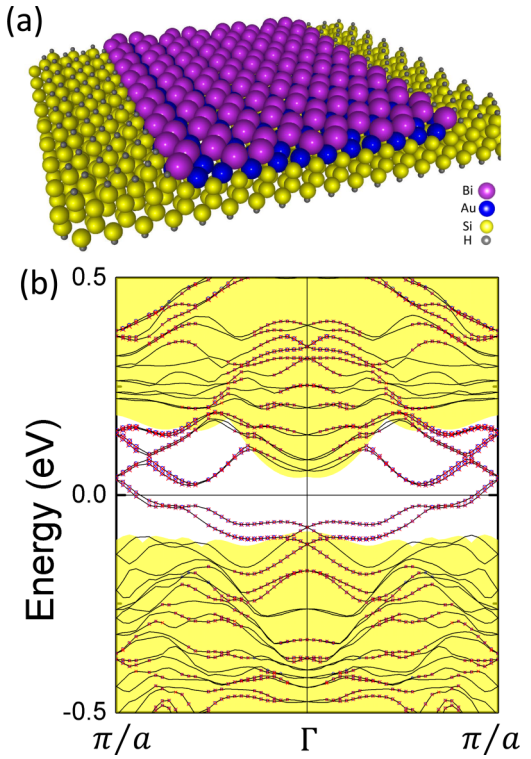

FIG. 3. (a) The structural model and (b) the band structure of a nanoribbon of 2/3 ML Bi on Au/Si(111)-$\sqrt{3}$ with a zigzag edge. The contribution from the edge on the right (left) hand side is marked with red crosses (blue circles); symbol sizes are proportional to the contribution from the Bi atoms on the edges. The yellow region denotes the projected bulk bands.

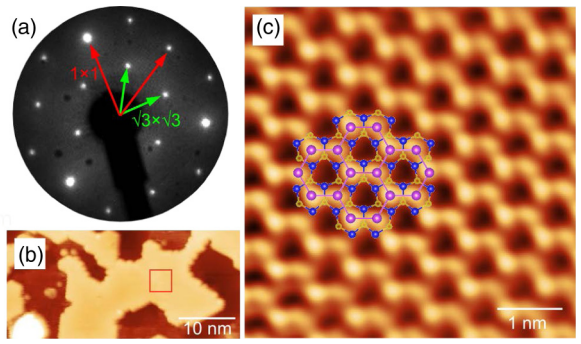

FIG. 4. Honeycomb pattern formed by depositing Bi at 2/3 ML on Au/Si(111)-$\sqrt{3}$. (a) LEED pattern taken at 48 eV with 1×1 and $\sqrt{3} \times \sqrt{3}$ lattice spots marked by red and green arrows, respectively. (b) 40×20 nm^2 STM image of 0.66 ML Bi on Au/Si(111)-$\sqrt{3}$ followed by annealing at ~ 280 °C. (c) Atom-resolved STM image of the area marked by the red square in (b). The image was acquired with a sample bias of 1.5 V at 0.1 nA. The honeycomb pattern and the $\sqrt{3} \times \sqrt{3}$ lattice are shown.

a clean Si(111) surface, which is passivated with H atoms, creating an interface between trivial and nontrivial states. In the band structure shown in Fig. 3(b), the bands resulting from the edge on the right (left) hand side are marked with red crosses (blue circles), with symbol sizes being proportional to the contributions of the Bi atoms on the edges. Our calculations show that for each type of edge, an odd number of edge states is seen to cross the Fermi level between Γ and π/a in Fig. 3(b), confirming that the system is a 2D TI; the small gap at π/a is due to the interaction between the two edges.

In order to obtain experimental support for our structural model and its stability, we have investigated a film with 0.66 ML Bi deposited on Au/Si(111)-$\sqrt{3}$ at room temperature, followed by postannealing at $\sim$280 °C, adapting the technique detailed in Ref. [47]. Upon Bi deposition, an additional sharp $\sqrt{3} \times \sqrt{3}$ LEED pattern was observed as shown in Fig. 4(a), indicating the appearance of an ordered structure on the surface. The corresponding topographic image obtained via STM [Fig. 4(b)] shows the presence of irregularly shaped flat islands with 0.316 ± 0.005 nm height, which are occasionally decorated with clusters. These clusters are likely the excess Bi which disappear at the higher annealing temperature ($\sim$280 °C), which is not high enough to desorb Au [56]. The STM image of the flat islands exhibits a clear honeycomb structure, in good accord with our predicted theoretical model in Fig. 4(c). Notably, the STM image shows that the honeycomb pattern is not completely planar, which is consistent with our theoretical finding that the buckled honeycomb pattern is slightly more stable than the planar case for group V adsorbates, although the system becomes trivial with buckling.

IV. CONCLUSIONS

By using first-principles computations, we have systematically examined the possibility of realizing nontrivial 2D topological phases via adsorption of metallic (nonmagnetic) elements from groups III to VI on the Au/Si(111)-$\sqrt{3}$ substrate. The formation of surface alloys with In, Tl, Ge, and Sn adsorbates is found to yield nontrivial phases with band gaps varying from 0 to 50 meV. Our LEED and STM experiments for Bi adsorbed on Au/Si(111)-$\sqrt{3}$ confirm the presence of a honeycomb pattern, in accord with our theoretical predictions. We hope that our study, which shows that Au/Si(111)-$\sqrt{3}$ could provide a viable platform for hosting 2D topological phases, including the possibility of tuning the topological state via gating (out-of-plane electric field) [14,29] and/or further doping of the surface, [37] will spur further experimental and theoretical work on this system.

ACKNOWLEDGMENTS

F.C.C. acknowledges support from the National Center for Theoretical Sciences and the Ministry of Science and Technology of Taiwan under Grants No. MOST-104-2112-M110-002-MY3 and No. MOST-101-2218-E-110-003-MY3. He is also grateful to the National Center for High-Performance Computing for computer time and facilities. C.C.K. acknowledges support from Ministry of Science and Technology of Taiwan under Grants No. MOST-102-2112-M-110-006-MY2 and No. MOST-104-2112-M-110-011. The work at Northeastern University was supported by the US Department of Energy (DOE), Office of Science, Basic Energy Sciences Grant No. DE-FG02-07ER46352 (core research), and benefited from Northeastern University's Advanced Scientific Computation Center (ASCC), the NERSC supercomputing center through DOE Grant No. DE-AC02-05CH11231, and support (applications to layered materials) from the DOE EFRC: Center for the Computational Design of Functional Layered Materials (CCDM) under Grant No. DE-SC0012575. H.L. acknowledges the Singapore National Research Foundation for support under NRF Award No. NRF-NRFF2013-03.

[1] C. L. Kane and E. J. Mele, Phys. Rev. Lett. **95**, 146802 (2005).
[2] B. A. Bernevig, T. L. Hughes, and S.-C. Zhang, Science **314**, 1757 (2006).
[3] M. König, S. Wiedmann, C. Brüne, A. Roth, H. Buhmann, L. W. Molenkamp, X.-L. Qi, and S.-C. Zhang, Science **318**, 766 (2007).
[4] A. Roth, C. Brüne, H. Buhmann, L. W. Molenkamp, J. Maciejko, X.-L. Qi, and S.-C. Zhang, Science **325**, 294 (2009).
[5] C. Liu, T. L. Hughes, X.-L. Qi, K. Wang, and S.-C. Zhang, Phys. Rev. Lett. **100**, 236601 (2008).
[6] I. Knez, R.-R. Du, and G. Sullivan, Phys. Rev. Lett. **107**, 136603 (2011).
[7] C. L. Kane and E. J. Mele, Phys. Rev. Lett. **95**, 226801 (2005).
[8] W.-F. Tsai, C.-Y. Huang, T.-R. Chang, H. Lin, H.-T. Jeng, and A. Bansil, Nat. Commun. **4**, 1500 (2013).

[9] C.-C. Liu, W. Feng, and Y. Yao, Phys. Rev. Lett. **107**, 076802 (2011).

[10] Y. Xu, B. Yan, H.-J. Zhang, J. Wang, G. Xu, P. Tang, W. Duan, and S.-C. Zhang, Phys. Rev. Lett. **111**, 136804 (2013).

[11] M. Wada, S. Murakami, F. Freimuth, and G. Bihlmayer, Phys. Rev. B **83**, 121310 (2011).

[12] F.-C. Chuang, L.-Z. Yao, Z.-Q. Huang, Y.-T. Liu, C.-H. Hsu, T. Das, H. Lin, and A. Bansil, Nano Lett. **14**, 2505 (2014).

[13] Z.-Q. Huang, C.-H. Hsu, F.-C. Chuang, Y.-T. Liu, H. Lin, W.-S. Su, V. Ozoliņš, and A. Bansil, New J. Phys. **16**, 105018 (2014).

[14] F.-C. Chuang, C.-H. Hsu, C.-Y. Chen, Z.-Q. Huang, V. Ozoliņš, H. Lin, and A. Bansil, Appl. Phys. Lett. **102**, 022424 (2013).

[15] J. O. Sofo, A. S. Chaudhari, and G. D. Barber, Phys. Rev. B **75**, 153401 (2007).

[16] D. C. Elias, R. R. Nair, T. M. G. Mohiuddin, S. V. Morozov, P. Blake, M. P. Halsall, A. C. Ferrari, D. W. Boukhvalov, M. I. Katsnelson, A. K. Geim *et al.*, Science **323**, 610 (2009).

[17] J. C. Garcia, D. B. de Lima, L. V. C. Assali, and J. F. Justo, J. Phys. Chem. C **115**, 13242 (2011).

[18] C. H. Zhang and S. S. Yan, J. Phys. Chem. C **116**, 4163 (2012).

[19] R. Wang, S. Wang, and X. Wu, J. Appl. Phys. **116**, 024303 (2014).

[20] L. Li, X. Zhang, X. Chen, and M. Zhao, Nano Lett. **15**, 1296 (2015).

[21] B.-H. Chou, Z.-Q. Huang, C.-H. Hsu, F.-C. Chuang, Y.-T. Liu, H. Lin, and A. Bansil, New J. Phys. **16**, 115008 (2014).

[22] C.-H. Hsu, Z.-Q. Huang, F.-C. Chuang, C.-C. Kuo, Y.-T. Liu, H. Lin, and A. Bansil, New J. Phys. **17**, 025005 (2015).

[23] C.-C. Liu, S. Guan, Z. Song, S. A. Yang, J. Yang, and Y. Yao, Phys. Rev. B **90**, 085431 (2014).

[24] Z. Song, C.-C. Liu, J. Yang, J. Han, M. Ye, B. Fu, Y. Yang, Q. Niu, J. Lu, and Y. Yao, NPG Asia Mater. **6**, e147 (2014).

[25] C. P. Crisostomo, L.-Z. Yao, Z.-Q. Huang, C.-H. Hsu, F.-C. Chuang, H. Lin, M. A. Albao, and A. Bansil, Nano Lett. **15**, 6568 (2015).

[26] L.-Z. Yao, C. P. Crisostomo, C.-C. Yeh, S.-M. Lai, Z.-Q. Huang, C.-H. Hsu, F.-C. Chuang, H. Lin, and A. Bansil, Sci. Rep. **5**, 15463 (2015).

[27] L. Chen, Z.-F. Wang, and F. Liu, Phys. Rev. B **87**, 235420 (2013).

[28] Z.-Q. Huang, F.-C. Chuang, C.-H. Hsu, Y.-T. Liu, H.-R. Chang, H. Lin, and A. Bansil, Phys. Rev. B **88**, 165301 (2013).

[29] Z.-Q. Huang, B.-H. Chou, C.-H. Hsu, F.-C. Chuang, H. Lin, and A. Bansil, Phys. Rev. B **90**, 245433 (2014).

[30] C. Sabater, D. Gosalbez-Martinez, J. Fernandez-Rossier, J. G. Rodrigo, C. Untiedt, and J. J. Palacios, Phys. Rev. Lett. **110**, 176802 (2013).

[31] M. C. Cottin, C. A. Bobisch, J. Schaffert, G. Jnawali, G. Bihlmayer, and R. Moller, Nano Lett. **13**, 2717 (2013).

[32] A. Takayama, T. Sato, S. Souma, T. Oguchi, and T. Takahashi, Nano Lett. **12**, 1776 (2012).

[33] T. Hirahara, G. Bihlmayer, Y. Sakamoto, M. Yamada, H. Miyazaki, S. I. Kimura, S. Blugel, and S. Hasegawa, Phys. Rev. Lett. **107**, 166801 (2011).

[34] F. Yang, L. Miao, Z.-F. Wang, M.-Y. Yao, F.-F. Zhu, Y.-R. Song, M.-X. Wang, J.-P. Xu, A. V. Fedorov, Z. Sun, G. B. Zhang, C.-H. Liu, F. Liu, D. Qian, C.-L. Gao, and J.-F. Jia, Phys. Rev. Lett. **109**, 016801 (2012).

[35] L. Miao, Z.-F. Wang, W.-M. Ming, M.-Y. Yao, M.-X. Wang, F. Yang, Y.-R. Song, F.-F. Zhu, A. V. Fedorov, Z. Sun, C.-L. Gao, C.-H. Liu, Q.-K. Xue, C.-X. Liu, F. Liu, D. Qian, and J.-F. Jia, Proc. Natl. Acad. Sci. USA **110**, 2758 (2013).

[36] Z.-F. Wang, M.-Y. Yao, W.-M. Ming, L. Miao, F.-F. Zhu, C.-H. Liu, C.-L. Gao, D. Qian, J.-F. Jia, and F. Liu, Nat. Commun. **4**, 1384 (2013).

[37] Y.-H. Lu, W.-T. Xu, M.-G. Zeng, G.-G. Yao, L. Shen, M. Yang, Z.-Y. Luo, F. Pan, K. Wu, T. Das, P. He, J.-Z. Jiang, J. Martin, Y.-P. Feng, H. Lin, and X.-S. Wang, Nano Lett. **15**, 80 (2015).

[38] M. Zhou, W.-M. Ming, Z. Liu, Z.-F. Wang, Y.-G. Yao, and F. Liu, Sci. Rep. **4**, 7102 (2014).

[39] M. Zhou, W. Ming, Z. Liu, Z.-F. Wang, P. Li, and F. Liu, Proc. Natl. Acad. Sci. USA **111**, 14378 (2014).

[40] I. Gierz, T. Suzuki, E. Frantzeskakis, S. Pons, S. Ostanin, A. Ernst, J. Henk, M. Grioni, K. Kern, and C. R. Ast, Phys. Rev. Lett. **103**, 046803 (2009).

[41] E. Frantzeskakis, S. Pons, and M. Grioni, Phys. Rev. B **82**, 085440 (2010).

[42] C.-H. Hsu, H.-R. Chang, F.-C. Chuang, Y.-T. Liu, Z.-Q. Huang, H. Lin, V. Ozoliņš, and A. Bansil, Surf. Sci. **626**, 68 (2014).

[43] D. V. Gruznev, I. N. Filippov, D. A. Olyanich, D. N. Chubenko, I. A. Kuyanov, A. A. Saranin, A. V. Zotov, and V. G. Lifshits, Phys. Rev. B **73**, 115335 (2006).

[44] D. V. Gruznev, A. V. Matetskiy, L. V. Bondarenko, E. A. Borisenko, D. A. Tsukanov, A. V. Zotov, and A. A. Saranin, Surf. Sci. **605**, 1420 (2011)

[45] J. K. Kim, K. S. Kim, J. L. McChesney, E. Rotenberg, H. N. Hwang, C. C. Hwang, and H. W. Yeom, Phys. Rev. B **80**, 075312 (2009)

[46] C.-H. Hsu, W.-H. Lin, V. Ozoliņš, and F.-C. Chuang, Phys. Rev. B **85**, 155401 (2012).

[47] S.-Y. Wu, C.-H. Hsu, W.-c. V. Yeh, H. Lin, F.-C. Chuang, and C.-C. Kuo, Phys. Rev. B **90**, 235407 (2014).

[48] J. P. Perdew, K. Burke, and M. Ernzerhof, Phys. Rev. Lett. **77**, 3865 (1996).

[49] P. Hohenberg, and W. Kohn, Phys. Rev. **136**, B864 (1964); W. Kohn, and L. J. Sham, *ibid.* **140**, A1133 (1965).

[50] G. Kresse and D. Joubert, Phys. Rev. B **59**, 1758 (1999).

[51] G. Kresse and J. Hafner, Phys. Rev. B **47**, 558 (1993); G. Kresse, and J. Furthmüller, *ibid.* **54**, 11169 (1996).

[52] H. J. Monkhorst and J. D. Pack, Phys. Rev. B **13**, 5188 (1976).

[53] T. Fukui and Y. Hatsugai, J. Phys. Soc. Jpn. **76**, 053702 (2007).

[54] A. Crepaldi, C. Tournier-Colletta, M. Pivetta, G. Autes, F. Patthey, H. Brune, O. V. Yazyev, and M. Grioni, Phys. Rev. B **88**, 195433 (2013).

[55] A. V. Krukau, O. A. Vydrov, A. F. Izmaylov, and G. E. Scuseria, J. Chem. Phys. **125**, 224106 (2006).

[56] T. Nagao, S. Hasegawa, K. Tsuchie, S. Ino, C. Voges, G. Klos, H. Pfnur, and M. Henzler, Phys. Rev. B **57**, 10100 (1998).